ACS APPLIED MATERIALS & INTERFACES

Research Article

Cite This: ACS Appl. Mater. Interfaces 2019, 11, 44241−44248

www.acsami.org

# Size-Controlled Growth of Silver Nanoparticles onto Functionalized Ordered Mesoporous Polymers for Efficient $CO_2$ Upgrading

Wei Zhang,[†,‡] Yu Mei,[†] Xiao Huang,[†] Peng Wu,[†] Haihong Wu,*[,†] and Mingyuan He[†]

[†]Shanghai Key Laboratory of Green Chemistry and Chemical Processes, School of Chemistry and Molecular Engineering, East China Normal University, 3663 North Zhongshan Road, Shanghai 200062, China

[‡]Van 't Hoff Institute for Molecular Sciences, University of Amsterdam, Science Park 904, Amsterdam 1098 XH, The Netherlands

*Supporting Information*

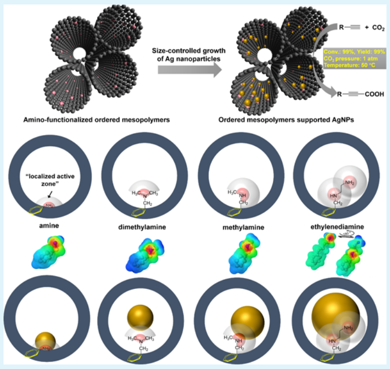

**ABSTRACT:** Highly dispersed metallic silver nanoparticles (AgNPs) are promising heterogeneous catalysts for carboxylative coupling of terminal alkynes with $CO_2$ under mild conditions. Yet, their size-controlled synthesis is very challenging because of the high surface energy. Here, we prepared a series of amino-functionalized ordered mesoporous polymers as hosts for anchoring AgNPs. Control experiments and computations showed that electron-rich amines were confined in mesochannels with varying electron density and steric hindrance, creating "localized active zones (LAZ)" to control the growth of AgNPs. The particle size of AgNPs grows along with the increased volume of LAZ around nitrogen species. We also revealed that the catalytic activity of Ag-based catalysts is size-dependent and increases with decreasing particle size. Building on these findings, we report a facile one-pot synthesis strategy for preparing an amine-incorporated ordered mesoporous polymer (NOMP) with a high specific surface area, small LAZ volume, and uniform amine sites with controllable loading. These features result in the formation of ultrasmall and monodispersed Ag nanoparticles. Remarkably, Ag@NOMP gave a quantitative target yield under the conditions of 1 atm $CO_2$ pressure and 50 °C, showing superior catalytic activity in $CO_2$ carboxylation compared to other mesoporous analogues.

**KEYWORDS:** *monodispersed silver, size-controlled synthesis, mesoporous materials, heterogeneous catalysis, $CO_2$ carboxylation*

## INTRODUCTION

The catalytic conversion of carbon dioxide ($CO_2$) into chemicals is an emerging strategy in green organic synthesis, reducing $CO_2$ emissions while also supplementing the carbon demand of the chemical industry.[1−3] Only a few feasible catalytic processes have been developed for using $CO_2$ as a starting material, not least because $CO_2$ is thermodynamically and kinetically stable.[4,5] The insertion of $CO_2$ into terminal alkynes via carboxylation is one of the most straightforward routes for producing alkynyl carboxylic acids,[6] which are key intermediates in the pharmaceutical and fine chemical sectors.[7] This route is more sustainable than the currently used hydrolysis of alkynyl bromides and carbonylation of alkynes as well as the transformation of expensive alkynyl metals.[8,9]

Silver (Ag)-based catalysts can efficiently catalyze this reaction,[10] as reported by the groups of Inoue,[11] Lu,[12,13] Gooßen,[14,15] Zhang,[16,17] He,[18] and Verpoort.[19,20] Yet, most of them are homogeneous Ag(I) complexes and salts, making it difficult for catalyst recovery and product separation.[10] To address this problem, Ag active species were immobilized on various solid supports, including poly-*N*-heterocyclic carbine,[16] solid Schiff base,[21] metal−organic frameworks (MOFs),[22−24] covalent organic frameworks,[25,26] hypercross-linked porous polymers,[27,28] and mesoporous oxides (MgO and $CeO_2$).[29,30] Among them, supported metallic Ag(0) nanoparticles (AgNPs) with high surface-to-volume ratios offer highly accessible active sites, showing remarkable catalytic performance toward $CO_2$ carboxylation. For example, Ma et al. reported MOF-supported AgNPs (Ag@MIL-101) for the highly efficient production of alkynyl carboxylic acids at ambient $CO_2$ pressure.[23] However, such ultrafine AgNPs tend to form aggregates because of the high surface energy, thereby lowering reactivity and durability.[31]

The encapsulation of AgNPs inside mesoporous materials (e.g., mesosilica and mesopolymers) is considered as an efficient strategy to suppress their growth and leaching, yielding well-dispersed and stable nanostructured catalysts.[32−36] Moreover, many studies showed that functional organic groups (such as amino and carboxyl groups) inside mesochannels can stabilize Ag species and enhance their dispersion.[37] Yet, the effect of these organic functionalities on nanostructuring AgNPs remains unclear. Understanding such an effect is crucial for designing size-controlled AgNPs in heterogeneous $CO_2$ catalysis.[38]

We now report that surface amine functionalities of mesoporous supports create localized active zones (LAZs) for controlling AgNP growth. Following our recent works on ordered mesoporous polymers (OMPs),[39−41] we introduced a

**Received:** August 23, 2019
**Accepted:** November 1, 2019
**Published:** November 1, 2019

DOI: 10.1021/acsami.9b14927
ACS Appl. Mater. Interfaces 2019, 11, 44241−44248

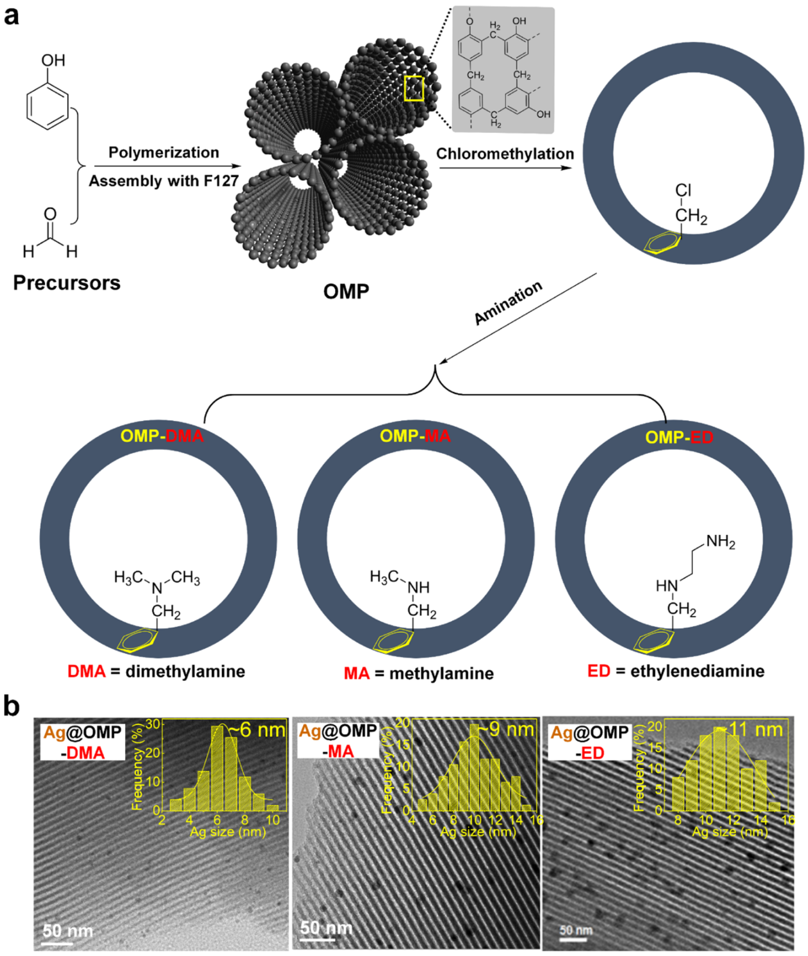

**Figure 1.** (a) Schematic illustration of the synthesis route of amino-functionalized OMPs (OMP−x, x = DMA, MA, and ED) via amination with three different amines: DMA, MA, and ED, respectively. (b) Representative HRTEM images of OMP−x; the insets give the particle size distribution of AgNPs.

set of amino groups into the OMPs that can facilitate the anchoring of AgNPs. More importantly, these functional species can alter the electronic and steric interactions with the Ag precursor, resulting in a size-controlled synthesis of AgNPs. Building on these results, we further report a one-pot strategy to prepare a new amino-functionalized OMP (NOMP), featuring a high surface area, high density of uniform amino sites, and robust organic mesostructures. The resulting NOMPs are ideal hosts for encapsulating mono-dispersed AgNPs with a mean size of ca. 4 nm. The Ag@NOMP showed high efficiency as a catalyst for the carboxylation of terminal alkynes with $CO_2$ under mild conditions, demonstrating an activity superior than other analogous amino-based OMP catalysts.

## ■ RESULTS AND DISCUSSION

**Catalyst Synthesis and Characterization of Amino-Functionalized OMPs.** Starting with an OMP as the support, we functionalized the surface with a set of amino groups by post treatment. Figure 1a briefly outlines the synthesis procedure. First, an FDU-type OMP (FDU stands for Fudan University) with a well-ordered two-dimensional (2D) hexagonal mesostructure was prepared by polycondensation of phenol with formaldehyde, following published procedures.[42] Subsequently, the amino groups were then introduced into the OMP material via a two-step process: chloromethylation of OMP and then amination of the chloromethylated ($-CH_2Cl$) OMP with a series of amines. Here, the OMP was modified with three different amines, namely, dimethylamine (DMA), methylamine (MA), and ethylenediamine (ED).[43] The resulting amino-functionalized OMPs are denoted as OMP−DMA, OMP−MA, and OMP−ED, respectively. They are employed as hosts to immobilize AgNPs via a simple impregnation−reduction method using silver nitrate ($AgNO_3$) as the precursor and methanol as the reduction agent, yielding amino-functionalized OMP-supported AgNPs (denoted as Ag@OMP−x, x = DMA, MA, and ED).

Small-angle X-ray diffraction (XRD) analysis shows that the highly ordered 2D hexagonal mesostructure of all Ag@OMP−x samples remained stable (Figure S1a). After the encapsulation of AgNPs inside the OMP, the diffraction peaks shifted to lower angles, in comparison with pure OMP. Both OMP−MA- and OMP−ED-supported AgNPs showed a set of new characteristic peaks at 38.2, 44.3, 64.5, and 77.5° (Figure S1b), which are attributed to the (111), (200), (220), and (311) planes of the face-centered cubic structure of metallic silver, respectively (JCPDS no. 04-0783).[44] The average crystalline sizes of AgNPs are calculated using the Debye−Scherrer formula on the basis of the width of (111) reflection,[45] decreasing as follows (see Table S1): Ag@OMP−ED (12.7 nm) > Ag@OMP−MA (10.2 nm) > Ag@OMP−DMA (7.5 nm). This trend matches well with our latter

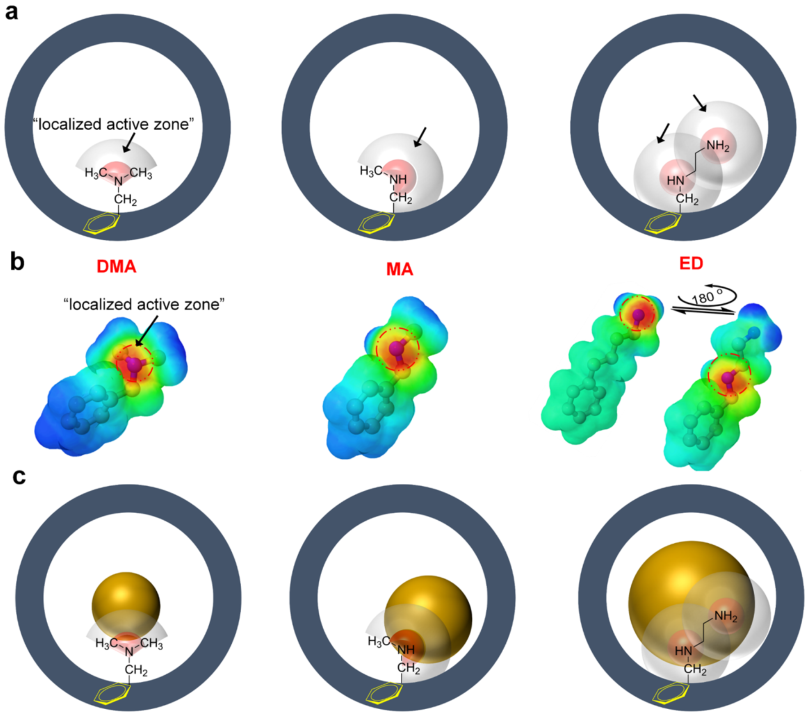

**Figure 2.** (a) Relative volume of the LAZ (gray) varies with the amino groups inside the OMP materials. (b) Comparison of the molecular electrostatic potentials of simplified amine models via CP2K. (c) Cartoon showing particle size of AgNPs increasing with an increase in the volume of LAZ around nitrogen atoms inside OMP−x.

transmission electron microscopy (TEM) study. The nitrogen ($N_2$) adsorption−desorption experiments for these Ag@OMP−x were performed (Figure S2). All of the samples showed a typical type IV isotherm with an H1-type hysteresis loop characteristic of a mesoporous polymer.[46] The pore diameters (inset in Figure S2) of all Ag-containing solids are identical to that of pure OMP, centered at ∼6.6 nm with a narrow distribution. Table S1 summarizes the corresponding porosity analysis and textural parameters, in which the surface area and pore volume of OMP−x decreased after the immobilization of AgNPs.

High-resolution TEM (HRTEM) provides direct evidence of the amino-induced growth of AgNPs. Figure 1b shows the representative HRTEM images of Ag@OMP−x samples viewed from the [100] direction, confirming AgNPs are homogeneously dispersed along the long-range ordered mesochannels.[40] For comparison, we prepared a pure OMP-supported metallic Ag under otherwise identical conditions (denoted as Ag@OMP). The HRTEM image of the amino-free Ag@OMP shows the formation of large Ag particles outside the mesopores (Figure S3). This indicates that the functionalization of the hydrophobic OMP surface with amino species can increase its wettability,[47] allowing for an aqueous solution of $AgNO_3$ into the hydrophobic channels.

Moreover, the amino groups can stabilize Ag precursors and turn the particle growth during the impregnation−reduction processes. The mean sizes of the AgNP nanoparticles in these series increased as follows: Ag@OMP−ED (11 nm) > Ag@OMP−MA (9 nm) > Ag@OMP−DMA (6 nm). This trend is in line with the deposition loadings of AgNPs (see Table S1), albeit all OMPs were loaded with equivalent amounts of amines (DMA 1.9 mmol/g, MA 2.1 mmol/g, and ED 2.0 mmol/g).[43] Therefore, we concluded that the size of the AgNPs closely depends on amine decoration. Note that one diamine molecule (−ED) has two nitrogen (N) atoms tethered together, and the N loading of OMP−ED is twice higher than that of monoamines (DMA and MA). This explains why OMP−ED enables large particle sizes of AgNPs with high loading. Intriguingly, the supported AgNPs were found to be sensitive to the structure of the monoamines, that is, the secondary amine-DMA tails on OMP gave a much smaller size of AgNPs (∼6 nm) than the primary amine-MA (∼9 nm).

On the basis of the above observations, we present an amino-induced hypothesis for describing the controllable growth of AgNPs inside ordered mesoporous channels (Figure 2). The amino group with a lone electron pair provides a strong electrostatic interaction with $Ag^+$ ions, and the active region of the interaction depends heavily on the amino species.[48,49] Here, we call this electron-rich region around nitrogen atoms as "LAZ", where the confined nucleation and growth of AgNPs occur.[50] As shown in Figure 2a, the LAZ can be tuned by the electron donor ability and steric hindrance of amino substituents. Obviously, DMA shows the smallest LAZ because of the steric hindrance of two methyl groups; the relative volumes of LAZ were ranked −ED > −MA > −DMA. This is in line with the calculated molecular electrostatic potentials of amine models via density functional theory calculations (Figure 2b).[48] The volume of LAZ is closely dependent on N's negative electrostatic potential, as the electronegative N atom creates a high electron density in a space. To simplify this, we built three models for DMA, MA, and ED, respectively, and compared their electrostatic potentials (a more detailed description of the simulations is provided in the Supporting Information). The values of electrostatic potentials in these models are −27 kJ/mol (DMA), −35 kJ/mol (MA), and −48 kJ/mol (ED), varying with the volume of LAZ. Increasing the volume of LAZ also increases the steric electron density, which in turn results in a

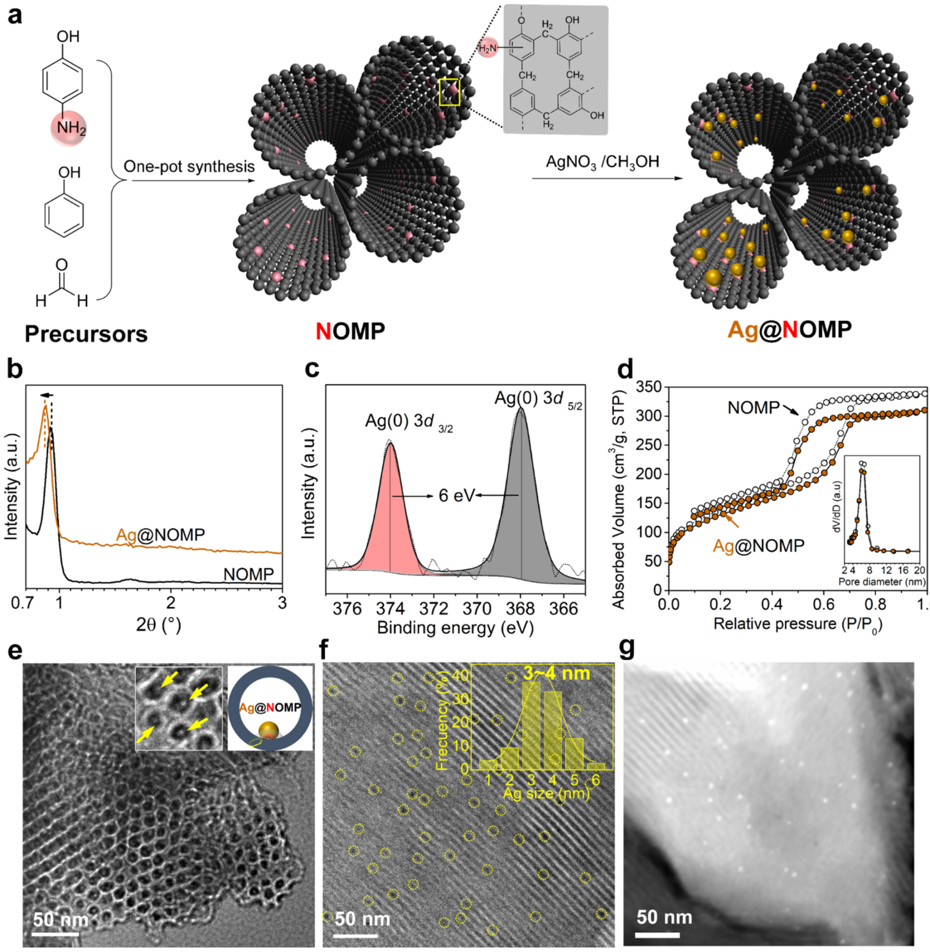

**Figure 3.** (a) Illustration of the one-pot synthesis route of amine-incorporated OMP (NOMP), followed by a simple impregnation−reduction to give Ag@NOMP. (b) Small-angle XRD patterns of NOMP and Ag@NOMP (the corresponding wide-angle XRD patterns are shown in Figure S9 in the Supporting Information). (c) High-resolution Ag 3d XPS spectra of Ag@NOMP. (d) Nitrogen adsorption−desorption isotherms and Barrett−Joyner−Halenda pore size distribution curves of NOMP and Ag@NOMP. (e,f) Representative HRTEM images of Ag@NOMP taken along the [110] and [100] directions. (g) HAADF−STEM image showing the well-dispersed AgNPs inside Ag@NOMP.

high trapping capacity of Ag ions, yielding large nanoparticles (Figure 2c). This trend is in line with the TEM results (cf. the size distributions of AgNPs in Figure 1b).

**Rational Design of Highly Dispersed AgNPs Encapsulated in an Amine-Incorporated OMP.** We then reasoned that the direct binding amine group ($-NH_2$) inside the OMP channels would lead to a confined LAZ, which in turn decreases the Ag size (Figure S4). To validate this, we developed a one-pot strategy for the controllable synthesis of $NH_2$-functionalized OMP (denoted as NOMP) via the direct coassembly of 4-aminophenol, phenol, and formaldehyde as starting materials in the presence of an amphiphilic triblock copolymer as a templating agent (Figure 3a). The Fourier transform infrared (FT-IR) (Figure S5), $^{13}C$ magic angle spinning nuclear magnetic resonance (MAS NMR) (Figure S6), and X-ray photoelectron spectroscopy (XPS) (Figure S7) spectra show the characteristic signals of $-NH_2$, confirming the successful synthesis of the targeted amine-containing mesopolymer. Moreover, the TEM images in Figure S8 exhibited the well-ordered 2D hexagonal morphology of NOMP. Next, the NOMP material was impregnated with an aqueous solution of $AgNO_3$ and then reduced by methanol to give Ag@NOMP (see the Experimental section in the Supporting Information for details).

The XRD patterns show that Ag@NOMP retained the well-ordered 2D hexagonal mesostructure (Figure 3b), accompanying the metallic Ag signal (see Figure S9). Moreover, Ag@NOMP only gave a weak (111) diffraction representing a smaller crystallite size, in comparison with Ag@OMP−DMA. The average crystalline sizes of AgNPs obtained from the (111) reflection were 6.1 and 7.5 nm for Ag@NOMP and Ag@OMP−DMA, respectively (Table S1). The XPS characterization also upholds the XRD results. As shown in Figure 3c, the Ag 3d spectra of Ag@NOMP can be fitted into two peaks located at 368.4 and 374.4 eV (with a spin energy separation of 6 eV), attributed to Ag $3d_{5/2}$ and Ag $3d_{3/2}$ of the metallic state of Ag(0), respectively.[51,52] To show how AgNPs interact with the amino species, the high-resolution XPS spectra of N 1s are measured in Figure S10. For NOMP, the spectra of N 1s were fitted with a symmetric peak centered at 399.7 eV, which can be attributed to the $-NH_2$ signal.[53] After introducing AgNPs, the binding energy corresponding to amino-N is shifted toward lower values (395 eV). This confirmed that Ag binds to $-NH_2$, decreasing the electron charge density of N species.[54,55] The $N_2$ sorption isotherms (Figure 3d) revealed that Ag@NOMP was mesoporous with a specific surface area of 456 $m^2/g$, comparable with the pristine NOMP (485 $m^2/g$). The corresponding textural parameters are summarized in Table S1.

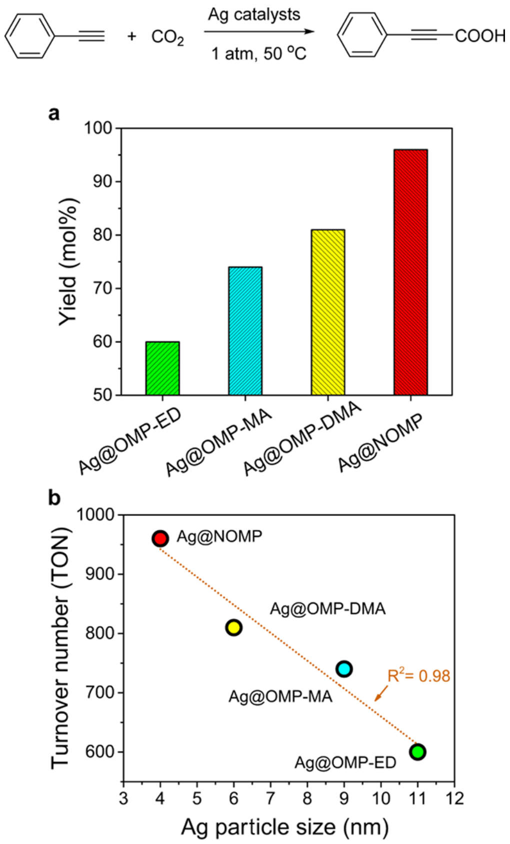

**Figure 4.** (a) Comparisons of carboxylation of EB with $CO_2$ to PA over various Ag-containing catalysts. (b) Plot for the correlation between the TON of PA produced on Ag catalysts and their particle sizes. Reaction conditions: EB (2.0 mmol), catalyst 0.1 mol % Ag-containing solid, $Cs_2CO_3$ (3 mmol), $CO_2$ (1.0 atm), 50 °C, dimethyl sulfoxide (DMSO) (15 mL), 12 h.

The HRTEM images of Ag@NOMP clearly show the dispersed and ultrasmall AgNPs inside mesochannels (Figure 3e,f). This is further evidenced by a high-angle annular dark-field scanning TEM (HAADF−STEM) image (Figure 3g), in which a large number of white dots can be observed corresponding to the homogeneously distributed Ag nanoparticles. Notably, in spite of a higher Ag loading (1.5 wt %), Ag@NOMP gave a much smaller particle size (ca. 4 nm, inset in Figure 3f) than Ag@OMP−DMA (ca. 6 nm with 0.26 wt %, see Table S1). These results confirmed further the importance of the confined LAZ effect.

**Catalytic Testing.** We studied the catalytic performance of these heterogeneous AgNP catalysts in the carboxylative coupling of 1-ethynylbenzene (EB) with $CO_2$ to phenylpropiolic acid (PA) at 50 °C under 1 atm $CO_2$ pressure. Control experiments confirmed that the reaction cannot proceed in the absence of catalysts or by just adding pristine amino-functionalized mesopolymer supports (OMP−x and NOMP). All Ag-containing samples showed good catalytic activity. As shown in Figure 4a, Ag@NOMP shows the best catalytic activity among all the catalysts tested in this series, giving a much higher yield of 96% than Ag@OMP−DMA (81%), Ag@OMP−MA (74%), and Ag@OMP−ED (60%). This is probably because Ag@NOMP features ultrasmall Ag sizes, thereby favoring the catalytic efficiency. To further evaluate the size-dependent catalytic performance, we plotted the turnover numbers (TONs, calculated as moles of PA produced per mole of Ag loading) against the corresponding particle sizes. Figure 4b exhibited a good linear correlation ($R^2$ = 0.98). This suggests that the carboxylation activity of the supported Ag catalysts depends closely on their particle sizes.

We further examined the catalytic scope of Ag@NOMP with 11 different terminal alkynes (Table 1). All the electron-donating (entries 1−3) and electron-withdrawing (entries 4−6) substituted phenylacetylenes were smoothly converted to the corresponding PAs with excellent yields (92−99%). Moreover, alkynes bearing the heteroaromatic-(2-ethynylthiophene, entry 7) and low polar aliphatic groups (entries 8−11) were tested, and they gave good target yields varying from 89 to 96%.

Recycling experiments were carried out for the Ag@NOMP catalyst. In each cycle, the Ag@NOMP solid was separated by simple filtration and washed with acetone and deionized water. Figure 5 shows that Ag@NOMP could be reused at least five times without significant loss of activity. Notably, despite the fact that the Ag content of the filtrate was below the detection limit of inductively coupled plasma-atomic emission spectroscopy analysis, a slight decrease in PA yield was observed at the fifth run. This probably comes from the partial oxidation of metallic Ag. This agrees well with the XPS results (Figure S11), where the Ag(I) peak was detected.[56] The TEM analysis (Figure S12) confirmed that the monodispersed Ag nanoparticles are stable without aggregation after reusing five times.

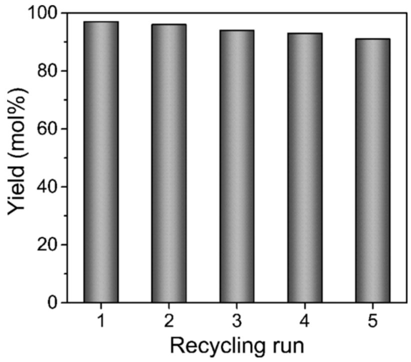

**Figure 5.** Recycling of the Ag@NOMP catalyst in the carboxylation of EB with $CO_2$ to PA.

All in all, our Ag@NOMP is among the best solid catalyst for the highly efficient conversion of $CO_2$ and terminal alkynes to alkynyl carboxylic acids.

## ■ CONCLUSIONS

In summary, we prepared a series of amino-decorated highly ordered mesopolymers for encapsulating metallic Ag nanoparticles and found that the amino groups control AgNP growth through "LAZs" surrounding electron-rich nitrogen atoms. The nature of LAZ is determined by the electron donor ability and steric hindrance of the amino substituent. As the volume of LAZ increases, more Ag species were trapped in this active region, resulting in the formation of undesired nonuniform large particles. With these findings at hand, we then developed a simple bottom-up route to the direct incorporation of $NH_2$ into the OMP framework (NOMP). Owing to its high surface area, uniform amine sites, and small LAZ size, NOMP was proven to be an ideal scaffold for stabilizing ultrasmall nanoparticles. The resulting Ag@NOMP

Table 1. Reaction Scope of Different Terminal Alkynes with $CO_2$ Over the Ag@NOMP Catalyst[a]

| Entry | Alkyne | Product | Yield (%) b |
|---|---|---|---|
| 1 | 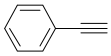 | 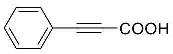 | 96 |
| 2 | 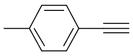 | 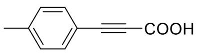 | 95 |
| 3 | 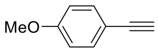 | 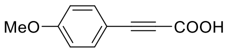 | 99 |
| 4 | 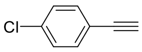 | 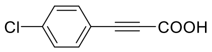 | 92 |
| 5 | 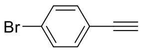 | 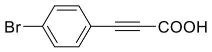 | 93 |
| 6 | 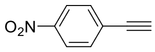 | 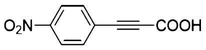 | 92 |
| 7 | 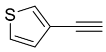 | 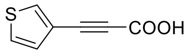 | 93 |
| 8 | 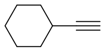 | 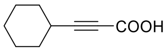 | 96 |
| 9 | 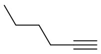 | 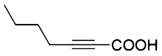 | 90 |
| 10 | 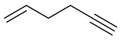 | 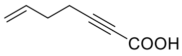 | 91 |
| 11 | 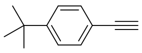 | 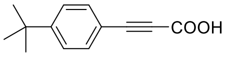 | 89 |

[a]Reaction conditions: alkyne (2.0 mmol), catalyst Ag@NOMP: 15 mg (0.1 mol % Ag), $Cs_2CO_3$ (3 mmol), $CO_2$ (1.0 atm), 50 °C, DMSO (15 mL), 12 h. [b]Isolated yields.

showed high efficiency in converting terminal alkynes and $CO_2$ into alkynyl carboxylic acids under mild conditions. In addition, size dependence was found for the metallic Ag-catalyzed carboxylation of $CO_2$. This work provides a facile approach for designing highly dispersed and stable metal nanoparticles for heterogeneous catalysis.

## ASSOCIATED CONTENT

### Supporting Information

The Supporting Information is available free of charge on the ACS Publications website at DOI: 10.1021/acsami.9b14927.

> Experimental procedures; computational details; additional characterization data of Ag@OMP−x and Ag@NOMP catalysts including XRD patterns, nitrogen adsorption−desorption isotherms, SEM/TEM images, FT-IR spectra, and $^{13}C$ MAS NMR spectra; and characterizations of reused catalyst (PDF)

## AUTHOR INFORMATION

### Corresponding Author

*E-mail: hhwu@chem.ecnu.edu.cn.

### ORCID

Wei Zhang: 0000-0003-4506-6583
Peng Wu: 0000-0003-2193-7356
Haihong Wu: 0000-0001-6266-8290

### Author Contributions

W.Z. and Y.M. contributed equally to this work.

### Notes

The authors declare no competing financial interest.

## ACKNOWLEDGMENTS

This work is supported by the National Natural Science Foundation of China (21573073), the National Key Research and Development Program of China (2017YFA0403102), and Shanghai Leading Academic Discipline Project (B409).

## REFERENCES

(1) He, M.; Sun, Y.; Han, B. Green Carbon Science: Scientific Basis for Integrating Carbon Resource Processing, Utilization, and Recycling. *Angew. Chem., Int. Ed.* **2013**, *52*, 9620−9633.

(2) Aresta, M.; Dibenedetto, A.; Angelini, A. Catalysis for the Valorization of Exhaust Carbon: from $CO_2$ to Chemicals, Materials, and Fuels. Technological Use of $CO_2$. *Chem. Rev.* **2014**, *114*, 1709−1742.

(3) Goeppert, A.; Czaun, M.; Jones, J.-P.; Surya Prakash, G. K.; Olah, G. A. Recycling of carbon dioxide to methanol and derived products—closing the loop. *Chem. Soc. Rev.* **2014**, *43*, 7995−8048.

(4) Zhou, W.; Cheng, K.; Kang, J.; Zhou, C.; Subramanian, V.; Zhang, Q.; Wang, Y. New horizon in C1 chemistry: breaking the selectivity limitation in transformation of syngas and hydrogenation of $CO_2$ into hydrocarbon chemicals and fuels. *Chem. Soc. Rev.* **2019**, *48*, 3193−3228.

(5) Artz, J.; Müller, T. E.; Thenert, K.; Kleinekorte, J.; Meys, R.; Sternberg, A.; Bardow, A.; Leitner, W. Sustainable Conversion of Carbon Dioxide: An Integrated Review of Catalysis and Life Cycle Assessment. *Chem. Rev.* **2018**, *118*, 434−504.

(6) Park, K.; Lee, S. Transition metal-catalyzed decarboxylative coupling reactions of alkynyl carboxylic acids. *RSC Adv.* **2013**, *3*, 14165−14182.

(7) Rodríguez, N.; Goossen, L. J. Decarboxylative coupling reactions: a modern strategy for C-C-bond formation. *Chem. Soc. Rev.* **2011**, *40*, 5030−5048.

(8) Yu, B.; Diao, Z.-F.; Guo, C.-X.; Zhong, C.-L.; He, L.-N.; Zhao, Y.-N.; Song, Q.-W.; Liu, A.-H.; Wang, J.-Q. Carboxylation of terminal alkynes at ambient $CO_2$ pressure in ethylene carbonate. *Green Chem.* **2013**, *15*, 2401−2407.

(9) Krief, A.; Kremer, A. Synthesis of Alkali Metal Carboxylates and Carboxylic Acids Using "Wet" and "Anhydrous" Alkali Metal Hydroxides. *Chem. Rev.* **2010**, *110*, 4772−4819.

(10) Fang, G.; Bi, X. Silver-catalysed reactions of alkynes: recent advances. *Chem. Soc. Rev.* **2015**, *44*, 8124−8173.

(11) Fukue, Y.; Oi, S.; Inoue, Y. Direct synthesis of alkyl 2-alkynoates from alk-1-ynes, $CO_2$, and bromoalkanes catalysed by copper(I) or silver(I) salt. *J. Chem. Soc., Chem. Commun.* **1994**, 2091.

(12) Zhang, X.; Zhang, W.-Z.; Ren, X.; Zhang, L.-L.; Lu, X.-B. Ligand-Free Ag(I)-Catalyzed Carboxylation of Terminal Alkynes with $CO_2$. *Org. Lett.* **2011**, *13*, 2402−2405.

(13) Zhang, X.; Zhang, W.-Z.; Shi, L.-L.; Zhu, C.; Jiang, J.-L.; Lu, X.-B. Ligand-free Ag(I)-catalyzed carboxylative coupling of terminal alkynes, chloride compounds, and $CO_2$. *Tetrahedron* **2012**, *68*, 9085−9089.

(14) Arndt, M.; Risto, E.; Krause, T.; Gooßen, L. J. C−H Carboxylation of Terminal Alkynes Catalyzed by Low Loadings of Silver(I)/DMSO at Ambient $CO_2$ Pressure. *ChemCatChem* **2012**, *4*, 484−487.

(15) Manjolinho, F.; Arndt, M.; Gooßen, K.; Gooßen, L. J. Catalytic C-H Carboxylation of Terminal Alkynes with Carbon Dioxide. *ACS Catal.* **2012**, *2*, 2014−2021.

(16) Yu, D.; Tan, M. X.; Zhang, Y. Carboxylation of Terminal Alkynes with Carbon Dioxide Catalyzed by Poly(N-Heterocyclic Carbene)-Supported Silver Nanoparticles. *Adv. Synth. Catal.* **2012**, *354*, 969−974.

(17) Yu, D.; Zhou, F.; Lim, D. S. W.; Su, H.; Zhang, Y. NHC-Ag/Pd-Catalyzed Reductive Carboxylation of Terminal Alkynes with $CO_2$ and $H_2$: A Combined Experimental and Computational Study for Fine-Tuned Selectivity. *ChemSusChem* **2017**, *10*, 836−841.

(18) Guo, C.-X.; Yu, B.; Xie, J.-N.; He, L.-N. Silver tungstate: a single-component bifunctional catalyst for carboxylation of terminal alkynes with $CO_2$ in ambient conditions. *Green Chem.* **2015**, *17*, 474−479.

(19) Díaz Velázquez, H.; Wu, Z.-X.; Vandichel, M.; Verpoort, F. Inserting $CO_2$ into Terminal Alkynes via Bis-(NHC)-Metal Complexes. *Catal. Lett.* **2017**, *147*, 463−471.

(20) Yuan, Y.; Xie, Y.; Zeng, C.; Song, D.; Chaemchuen, S.; Chen, C.; Verpoort, F. A simple and robust AgI/KOAc catalytic system for the carboxylative assembly of propargyl alcohols and carbon dioxide at atmospheric pressure. *Catal. Sci. Technol.* **2017**, *7*, 2935−2939.

(21) Wu, Z.; Sun, L.; Liu, Q.; Yang, X.; Ye, X.; Hu, Y.; Huang, Y. A Schiff base-modified silver catalyst for efficient fixation of $CO_2$ as carboxylic acid at ambient pressure. *Green Chem.* **2017**, *19*, 2080−2085.

(22) Molla, R. A.; Ghosh, K.; Banerjee, B.; Iqubal, M. A.; Kundu, S. K.; Islam, S. M.; Bhaumik, A. Silver nanoparticles embedded over porous metal organic frameworks for carbon dioxide fixation via carboxylation of terminal alkynes at ambient pressure. *J. Colloid Interface Sci.* **2016**, *477*, 220−229.

(23) Liu, X.-H.; Ma, J.-G.; Niu, Z.; Yang, G.-M.; Cheng, P. An Efficient Nanoscale Heterogeneous Catalyst for the Capture and Conversion of Carbon Dioxide at Ambient Pressure. *Angew. Chem., Int. Ed.* **2015**, *54*, 988−991.

(24) Zhu, N.-N.; Liu, X.-H.; Li, T.; Ma, J.-G.; Cheng, P.; Yang, G.-M. Composite System of Ag Nanoparticles and Metal-Organic Frameworks for the Capture and Conversion of Carbon Dioxide under Mild Conditions. *Inorg. Chem.* **2017**, *56*, 3414−3420.

(25) Lan, X.; Du, C.; Cao, L.; She, T.; Li, Y.; Bai, G. Ultrafine Ag Nanoparticles Encapsulated by Covalent Triazine Framework Nanosheets for $CO_2$ Conversion. *ACS Appl. Mater. Interfaces* **2018**, *10*, 38953−38962.

(26) Dang, Q.-Q.; Liu, C.-Y.; Wang, X.-M.; Zhang, X.-M. Novel Covalent Triazine Framework for High-Performance $CO_2$ Capture and Alkyne Carboxylation Reaction. *ACS Appl. Mater. Interfaces* **2018**, *10*, 27972−27978.

(27) Modak, A.; Bhanja, P.; Bhaumik, A. Microporous Nanotubes and Nanospheres with Iron-Catechol Sites: Efficient Lewis Acid Catalyst and Support for Ag Nanoparticles in CO2 Fixation Reaction. *Chem.—Eur. J.* **2018**, *24*, 14189−14197.

(28) Wu, Z.; Liu, Q.; Yang, X.; Ye, X.; Duan, H.; Zhang, J.; Zhao, B.; Huang, Y. Knitting Aryl Network Polymers-Incorporated Ag Nanoparticles: A Mild and Efficient Catalyst for the Fixation of $CO_2$ as Carboxylic Acid. *ACS Sustainable Chem. Eng.* **2017**, *5*, 9634−9639.

(29) Chowdhury, A. H.; Ghosh, S.; Islam, S. M. Flower-like AgNPs@m-MgO as an excellent catalyst for $CO_2$ fixation and acylation reactions under ambient conditions. *New J. Chem.* **2018**, *42*, 14194−14202.

(30) Zhang, X.; Wang, D.; Jing, M.; Liu, J.; Zhao, Z.; Xu, G.; Song, W.; Wei, Y.; Sun, Y. Ordered Mesoporous $CeO_2$-supported Ag as an Effective Catalyst for Carboxylative Coupling Reaction Using $CO_2$. *ChemCatChem* **2019**, *11*, 2089−2098.

(31) Fiévet, F.; Ammar-Merah, S.; Brayner, R.; Chau, F.; Giraud, M.; Mammeri, F.; Peron, J.; Piquemal, J.-Y.; Sicard, L.; Viau, G. The polyol process: a unique method for easy access to metal nanoparticles with tailored sizes, shapes and compositions. *Chem. Soc. Rev.* **2018**, *47*, 5187−5233.

(32) Liu, X.; Jin, R.; Chen, D.; Chen, L.; Xing, S.; Xing, H.; Xing, Y.; Su, Z. In situ assembly of monodispersed Ag nanoparticles in the channels of ordered mesopolymers as a highly active and reusable hydrogenation catalyst. *J. Mater. Chem. A* **2015**, *3*, 4307−4313.

(33) Saikia, D.; Huang, Y.-Y.; Wu, C.-E.; Kao, H.-M. Size dependence of silver nanoparticles in carboxylic acid functionalized mesoporous silica SBA-15 for catalytic reduction of 4-nitrophenol. *RSC Adv.* **2016**, *6*, 35167−35176.

(34) Sun, Z.; Li, H.; Cui, G.; Tian, Y.; Yan, S. Multifunctional magnetic core-shell dendritic mesoporous silica nanospheres decorated with tiny Ag nanoparticles as a highly active heterogeneous catalyst. *Appl. Surf. Sci.* **2016**, *360*, 252−262.

(35) Fujiwara, K.; Kuwahara, Y.; Sumida, Y.; Yamashita, H. Synthesis of Ag nanoparticles encapsulated in hollow silica spheres for efficient and selective removal of low-concentrated sulfur compounds. *J. Mater. Chem. A* **2017**, *5*, 25431−25437.

(36) Fan, H.-T.; Liu, X.-G.; Xing, X.-J.; Li, B.; Wang, K.; Chen, S.-T.; Wu, Z.; Qiu, D.-F. Ordered mesoporous silica cubic particles decorated with silver nanoparticles: a highly active and recyclable heterogeneous catalyst for the reduction of 4-nitrophenol. *Dalton Trans.* **2019**, *48*, 2692−2700.

(37) Kang, H.; Buchman, J. T.; Rodriguez, R. S.; Ring, H. L.; He, J.; Bantz, K. C.; Haynes, C. L. Stabilization of Silver and Gold Nanoparticles: Preservation and Improvement of Plasmonic Functionalities. *Chem. Rev.* **2019**, *119*, 664−699.

(38) Lu, S.; Hu, Y.; Wan, S.; McCaffrey, R.; Jin, Y.; Gu, H.; Zhang, W. Synthesis of Ultrafine and Highly Dispersed Metal Nanoparticles Confined in a Thioether-Containing Covalent Organic Framework and Their Catalytic Applications. *J. Am. Chem. Soc.* **2017**, *139*, 17082−17088.

(39) Zhang, W.; Liu, T.; Wu, H.; Wu, P.; He, M. Direct synthesis of ordered imidazolyl-functionalized mesoporous polymers for efficient chemical fixation of $CO_2$. *Chem. Commun.* **2015**, *51*, 682−684.

(40) Zhang, W.; Mei, Y.; Wu, P.; Wu, H.-H.; He, M.-Y. Highly tunable periodic imidazole-based mesoporous polymers as cooperative catalysts for efficient carbon dioxide fixation. *Catal. Sci. Technol.* **2019**, *9*, 1030−1038.

(41) Xing, R.; Liu, N.; Liu, Y.; Wu, H.; Jiang, Y.; Chen, L.; He, M.; Wu, P. Novel Solid Acid Catalysts: Sulfonic Acid Group-Function-

alized Mesostructured Polymers. *Adv. Funct. Mater.* **2007**, *17*, 2455−2461.

(42) Zhang, W.; Wang, Q.; Wu, H.; Wu, P.; He, M. A highly ordered mesoporous polymer supported imidazolium-based ionic liquid: an efficient catalyst for cycloaddition of $CO_2$ with epoxides to produce cyclic carbonates. *Green Chem.* **2014**, *16*, 4767−4774.

(43) Xing, R.; Wu, H.; Li, X.; Zhao, Z.; Liu, Y.; Chen, L.; Wu, P. Mesopolymer solid base catalysts with variable basicity: preparation and catalytic properties. *J. Mater. Chem.* **2009**, *19*, 4004−4011.

(44) Yamamoto, M.; Nakamoto, M. Novel preparation of monodispersed silver nanoparticles via amine adducts derived from insoluble silver myristate in tertiary alkylamine. *J. Mater. Chem.* **2003**, *13*, 2064−2065.

(45) Biju, V.; Sugathan, N.; Vrinda, V.; Salini, S. L. Estimation of lattice strain in nanocrystalline silver from X-ray diffraction line broadening. *J. Mater. Sci.* **2008**, *43*, 1175−1179.

(46) Meng, Y.; Gu, D.; Zhang, F.; Shi, Y.; Yang, H.; Li, Z.; Yu, C.; Tu, B.; Zhao, D. Ordered Mesoporous Polymers and Homologous Carbon Frameworks: Amphiphilic Surfactant Templating and Direct Transformation. *Angew. Chem., Int. Ed.* **2005**, *117*, 7215−7221.

(47) Wiener, C. G.; Qiang, Z.; Xia, Y.; Tyagi, M.; Vogt, B. D. Impact of surface wettability on dynamics of supercooled water confined in nitrogen-doped ordered mesoporous carbon. *Phys. Chem. Chem. Phys.* **2018**, *20*, 28019−28025.

(48) Zhang, W.; Ensing, B.; Rothenberg, G.; Raveendran Shiju, N. Designing effective solid catalysts for biomass conversion: Aerobic oxidation of ethyl lactate to ethyl pyruvate. *Green Chem.* **2018**, *20*, 1866−1873.

(49) Zhang, W.; Innocenti, G.; Oulego, P.; Gitis, V.; Wu, H.; Ensing, B.; Cavani, F.; Rothenberg, G.; Shiju, N. R. Highly Selective Oxidation of Ethyl Lactate to Ethyl Pyruvate Catalyzed by Mesoporous Vanadia-Titania. *ACS Catal.* **2018**, *8*, 2365−2374.

(50) Slot, T. K.; Eisenberg, D.; Rothenberg, G. Cooperative Surface-Particle Catalysis: The Role of the ″Active Doughnut″ in Catalytic Oxidation. *ChemCatChem* **2018**, *10*, 2119−2124.

(51) Wang, N.; Guan, B.; Zhao, Y.; Zou, Y.; Geng, G.; Chen, P.; Wang, F.; Liu, M. Sub-10 nm Ag Nanoparticles/Graphene Oxide: Controllable Synthesis, Size-Dependent and Extremely Ultrahigh Catalytic Activity. *Small* **2019**, *15*, 1901701.

(52) Sun, L.; Zhang, D.; Sun, Y.; Wang, S.; Cai, J. Facile Fabrication of Highly Dispersed Pd@Ag Core-Shell Nanoparticles Embedded in Spirulina platensis by Electroless Deposition and Their Catalytic Properties. *Adv. Funct. Mater.* **2018**, *28*, 1707231.

(53) Lai, L.; Chen, L.; Zhan, D.; Sun, L.; Liu, J.; Lim, S. H.; Poh, C. K.; Shen, Z.; Lin, J. One-step synthesis of $NH_2$-graphene from in situ graphene-oxide reduction and its improved electrochemical properties. *Carbon* **2011**, *49*, 3250−3257.

(54) Zhou, R.; Qiao, S. Z. Silver/Nitrogen-Doped Graphene Interaction and Its Effect on Electrocatalytic Oxygen Reduction. *Chem. Mater.* **2014**, *26*, 5868−5873.

(55) Zhang, W.; Oulego, P.; Slot, T. K.; Rothenberg, G.; Shiju, N. R. Selective Aerobic Oxidation of Lactate to Pyruvate Catalyzed by Vanadium-Nitrogen-Doped Carbon Nanosheets. *ChemCatChem* **2019**, *11*, 3381−3387.

(56) Li, B.; Wang, H.; Zhang, B.; Hu, P.; Chen, C.; Guo, L. Facile Synthesis of One Dimensional AgBr@Ag Nanostructures and Their Visible Light Photocatalytic Properties. *ACS Appl. Mater. Interfaces* **2013**, *5*, 12283−12287.